

Computational Analysis of Flow Field on Cross-Flow Hydro Turbines

Warjito, Budiarmo, and Dendy Adanta, *Member IAENG*

Abstract— A better understanding of the flow field of the cross-flow turbine (CFT) will be useful in its design and operation. As far as is known, no comprehensive study carried out relating to the effect of Reynolds number to turbulent shear stress, shear wall, energy kinetic turbulent, dissipation rate and Reynolds stress, and the occurrence of vortices around the runners of the CFTs. This study was designed to investigate the flow field in the nozzle and runner of the CFT using computational fluid dynamics (CFD) method. CFD methods were chosen because they can visualize detailed flow patterns that other methods cannot. The setups used in the CFD method such as two-dimensional unsteady simulations, six degrees of freedom features, shear stress transport $k-\omega$ turbulent model, and pressure-based solver. Based on results, for the nozzle, the shape of the velocity profile shows that the highest momentum flux occurs at the end of the nozzle, near the runner. Distribution of shear wall was highest at the base and tip of the nozzle; it was lowest at the centre. The turbulent kinetic energy profile at the nozzle was proportional to the turbulent boundary layer profile, Reynolds stress and eddy viscosity. This indicated that nozzle shape affects the momentum flux; therefore, good nozzle geometry can transfer the maximum water energy into the blade. The nozzle's optimum geometry can be achieved by discharge and direction, optimizing velocity magnitude. This minimizes energy loss due to friction between the stream, vortex and mass of wasted fluid. For the runner, the highest turbulent kinetic energy, dissipation rate and Reynolds stress were located at the runner. Not all the water's energy converted into mechanic energy because the part of that energy was used in mixing between water and air. The establishment of lift force on the active blades was not caused by the flow field that crosses the upper part of the blade, but by the momentum of water that hit the lower part of the blade. A vortex formed due to separation of the flow from the blade significantly affected the runner's performance rather than rotational flow (air phase) in the CFT.

Index Terms—Computational, cross-flow turbine, flow field, turbulence flow.

Manuscript received May 07, 2020; revised October 27, 2020. This work was supported by the Ministry of Research, Technology and Higher Education (KEMENRISTEK DIKTI) of the Republic of Indonesia with grant No: NKB-1746/UN2.R3.1/HKP.05.00/2019.

Warjito is with the Department of Mechanical Engineering, Faculty of Engineering, Universitas Indonesia, Depok 16424, West Java, Indonesia (e-mail: warjito@eng.ui.ac.id).

Budiarmo is with the Department of Mechanical Engineering, Faculty of Engineering, Universitas Indonesia, Depok 16424, West Java, Indonesia (e-mail: budiarmo@ui.ac.id).

Dendy Adanta is with the Department of Mechanical Engineering, Faculty of Engineering, Universitas Sriwijaya, Indralaya 30662, South Sumatera, Indonesia (corresponding author to provide phone: +62-711-580-272; fax: +62-711-580-272; e-mail: dendyadanta@gmail.com).

I. INTRODUCTION

HYDROPOWER turbines can be used as independent power plants for remote areas that have water energy potential, and they are often more suitable for such areas than wind turbines, or solar photovoltaics (PV) [1]. Besides, per kW of hydropower turbine has higher life-cycle cost than wind turbines and solar PV [2]. Remote areas in several developing countries, such as Cameroon, Nepal, Rwanda, Honduras, Bolivia, and Peru, use hydropower turbines as independent power plants [3].

When considering the characteristics of simple design, modularity, and portability, the CFTs are more suitable for independent power plants in remote areas than Turgo, Pelton, propeller, or waterwheel turbines [4]. Furthermore, the efficiency of the CFT is more stable because it can work under high discharge deviations [5], [6]. The mechanical efficiency of CFTs is 50% to 80% [7], [8].

A the CFT is a type of impulse turbine which absorbs kinetic energy from water to rotate the shaft [1], [3], [9]. The CFTs generally consist of two main components: nozzle and runner. The nozzle function changes the potential energy of water to kinetic and water velocity rectifier, and the runner function changes the kinetic energy of water to mechanic energy [10]. A comprehensive study of the nozzle and runner design procedures to achieve efficiency in the 90% range has been done [11]. In this study, the known relationship was between the design of the nozzle and the best shape of the blade. The CFT runners absorb the energy of water in the first and second stage [12]; this has been proven both computationally [10], [13] and experimentally [12]. The ideal (optimum) condition for energy absorption in the first stage and the second stage is 70% and 30%, respectively [1]. Furthermore, there are two important parameters of the runner that affect the power generated: the number of blades (z) and absolute angle of attack (α) [14]. Determination of the number of blades is important because too many blades will increase losses, weight and investment cost, but too few cause higher losses from flow separation on the outlet of the blade in both the first and second stage [14]. The consideration of the absolute angle of attack is important because it will affect the theory of velocity triangle which greatly influences power predictions [14]. On other hand, the α and β angle (absolute and relative angle of attack) are dependent on the blade shape; therefore, the effect of blade depth also must be considered. A recent analysis states that blade depth has an influence on the performance of CFT [1]. Meanwhile, the experimental results found that mechanical efficiency reached 80% using guide vanes [15], [16]. However, when guide vanes are not

used, efficiency increases 5 to 10% [10], [17].

Studies related to the flow physics phenomenon also cover some of the major themes of the CFT research such as the concept of a reaction turbine [16], in which turbine efficiency increases when a draft tube is used because it reduces some undesirable phenomena such as backflow and vortex. To ensure the reaction turbine concept can be applied to the CFTs, an experiment with simulated the CFT blades using aerofoil NACA 6509 and 6712 was carried out, and it was concluded that curvature-shaped blades produced higher efficiency than the NACA 6509 and 6712 aerofoil. The results of this experiment indicated that the CFTs cannot use the concept of reaction turbines [9]. Moreover, there is no contribution to the lift force in the energy conversion process [9]. Besides, the flow field caused the runner to work abnormally because of recirculation and, finally, increased losses [1], [9], [18]. Though wide-ranging, none of the above studies have been able to give detailed explanations of the energy transfer process and the causes of flow losses, or how to overcome losses.

Computational fluid dynamics (CFD) method can be used to uncover the flow physics phenomena such as the recirculation flow that occurs in internal runners, losses due to the shape of the nozzle and or blade, as well as the process of changing momentum. In fact, there have been many studies on physical phenomenon, and many phenomena can be explained properly. As far as is known, no comprehensive study carried out relating to the effect of Reynolds number (Re) to turbulent shear stress (τ_{turb}), wall stress (τ_{wall}), energy kinetic turbulent (k), dissipation rate (ϵ) and Reynolds stress (Re_{stress}), and the occurrence of vortices around the runners of the CFTs. These flow fields are very important in the CFTs, and a better understanding of them will be useful in their design and operation. Thus, this study was designed to investigate the flow field in the nozzle and runner of the CFT using CFD methods. CFD simulations were chosen because they can visualize detailed flow patterns that other methods cannot [1].

II. METHODS

Before running computations, several processes must be completed, such as the determination of the turbine geometry, simulation setup with the determination of boundary conditions, and independence testing.

A. Turbine Geometry

The present work continues research reported previously, and the details about the comprehensive calculation of dimensions are discussed elsewhere [1], [9], [19]. The geometry specified in Table 1 is illustrated in Fig. 1.

B. Simulation Setup

After determining the geometry parameters (Table 1), the geometry is then built by computer-aided design (CAD) software to be simulated in ANSYS™ FLUENT® 18.2 Academic version. Two-dimensional (2D) transient domains represent the actual performance (efficiency) of the CFT with an error of 1.5% when compared with experimental

TABLE I
THE CFT PARAMETERS DESIGN

Symbols	Descriptions	Unit
D	Outer diameter	161 mm
d	Inner diameter	104 mm
S_0	Nozzle height	47 mm
B	Nozzle width	99 mm
W	Turbine width	139 mm
R_b	Blade curve radius	29.8 mm
α	Angle of attack	22°
β_1	Blade angle outlet	39°
β_2	Blade angle outlet	90°
λ	Inlet discharge angle	90°
δ	Blade angle curvature	62.6°
z	Number of blades	35

results [3], [9]. This study uses a dynamic mesh with six-degrees of freedom (6-DoF) feature because the rotation of the runner is a computational result not a boundary condition, so that the flow pattern that will occur is more precise than the moving mesh. Then, simulations were run with ten variations inlet of pressure, from 98.1 kPa until 981 kPa which will later be referred to as the Reynolds number (Re).

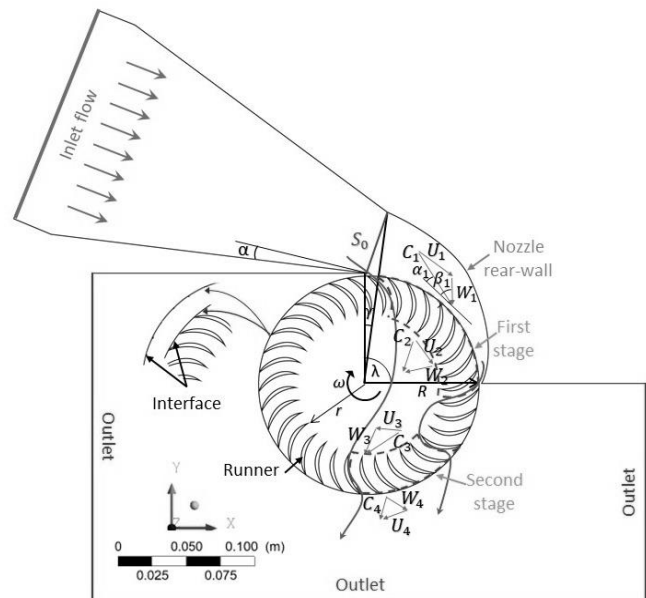


Fig. 1. Geometry and parameters of the CFT (redrawing from previous study [1], [9])

Several pre-processing steps must be applied. First, the geometrical dimensions must be identified, such as the determination of inlet, outlet, wall, runner, and interface. Second, after these dimensions are identified, the runner and turbine house interfaces are joined (see Fig. 1 in part of the interface) to avoid the calculation being an error—if this is not specified, the ANSYS FLUENT will consider the interface as a wall. Third, the geometrical dimensions are quantized into a mesh. Fourth, is the determination of boundary condition. A solver-type pressure base is chosen because of the flow used as an incompressible flow. The governing equation of the continuity equation in Cartesian coordinates for incompressible flow is

$$\frac{\partial}{\partial x_i}(\rho u_j) \quad (1)$$

The Reynolds Average Navier–Stokes (RANS) with body forces is

$$\frac{\partial \rho u_i}{\partial t} + \frac{\partial \rho u_i u_j}{\partial x_j} = -\frac{\partial p}{\partial x_i} + \frac{\partial}{\partial x_j} (\overline{\tau_{ij}} - \overline{\rho u'_i u'_j}) + \rho g_j \quad (2)$$

where u is the local average flow velocity, u' is the average local velocity fluctuation, g is the acceleration due to gravity, ρ is density, τ_{ij} is the viscous stress tensor, and $-\rho u'_i u'_j$ is the Reynolds stress tensor. This study assumes a body force that influences the energy conversion process, and as seen in Fig. 1, g is given in the direction of y with a value of -9.81 m/s^2 ; $g_j = -9.81 \text{ m/s}^2$. Computations were run using volume of fluid (VoF) multiphase modelling with the constant interfacial surface tension of $0.0728 \text{ N}\cdot\text{m}$. Water was considered as the fluid in the turbine, so the volume fraction of water in the inlet was set to 1 and the volume fraction of air was set to 0, meaning that no air accompanies water in the inlet. At the outlet, the volume fraction of air is set to 1. The backflow setting of the air phase must be set to 1 to ensure there is no water get in except the inlet. The continuity equation for this volume of fluid (VoF) model is given in (3) [20].

$$\frac{\partial}{\partial t} (\alpha_n \rho_n) + \frac{\partial}{\partial x_j} (\alpha_n \rho_n u_{j,n}) = \frac{1}{V} \sum_{m=1}^{\text{all phase}} (\dot{m}_{mn} - \dot{m}_{nm}) \quad (3)$$

where \dot{m}_{mn} is the mass transfer of both phases.

The Boussinesq hypothesis in (4) relates the Reynolds stress tensor to the mean velocity gradient. The Reynolds stress tensor ($-\rho u'_i u'_j$) must be modelled appropriately when using the RANS approach [21][22].

$$-\overline{\rho u'_i u'_j} = \mu_t \left(\frac{\partial u_i}{\partial x_j} + \frac{\partial u_j}{\partial x_i} \right) - \frac{2}{3} \left(\rho k + \mu_t \frac{\partial u_i}{\partial x_i} \right) \delta_{ij} \quad (4)$$

where μ_t is the turbulence or eddy viscosity, δ_{ij} is the Kronecker delta, and k is the turbulent kinetic energy. The surfaces set as interfaces are joined using rotation and re-meshing. Then, smoothing is applied to repair and improve the mesh resolution owing to changes in size caused by the rotating runner. The 6-DoF feature is activated using preloading and the moment of inertia. The preloading is the minimum torque needed to rotate the runner, and is equal to the accumulation of load from friction and the attached generator and the moment of inertia, which can be determined from the CAD model.

Previous studies have investigated the turbulent flow patterns in the CFT. Based on the assessment of six turbulence models suitable for the simulation of the CFTs with three criteria (error of numerical results, average iteration timestep, and relative average calculation timestep), the recommended turbulent model is the standard transition shear-stress-transport (SST) model with k - ω equations [3]. The SST k - ω equations are as follows [21], [22].

for k :

$$\frac{\partial (\rho k)}{\partial t} + \frac{\partial (\rho k u_j)}{\partial x_j} = \frac{\partial}{\partial x_i} \left(\Gamma_k \frac{\partial k}{\partial x_j} \right) + G_k - Y_k + S_k \quad (5)$$

for ω :

$$\frac{\partial (\rho \omega)}{\partial t} + \frac{\partial (\rho \omega u_j)}{\partial x_j} = \frac{\partial}{\partial x_i} \left(\Gamma_\omega \frac{\partial \omega}{\partial x_j} \right) + G_\omega - Y_\omega + S_\omega \quad (6)$$

where Γ_k and Γ_ω are the effective diffusivity, G_k and G_ω are the productions of k or ω , Y_k and Y_ω are the dissipation of k or ω , and S_k and S_ω are user-defined source terms [21][22].

C. Independency Test Method

After pre- and post-processing is determined, independence testing is needed to verify the simulation. Independence tests were conducted to find the lowest amount of accumulated calculation errors and rounding that could be produced. Two variables were varied in the independence test: the timestep and mesh resolution. To determine the best timestep, we analysed three timestep frequencies: 500 Hz, 1250 Hz, and 2500 Hz, which are equivalent to timesteps of 0.001 s, 0.0008 s, 0.0005 s, and 0.0004 s, respectively.

Mesh resolution independence was tested with three different numbers of mesh elements: coarse (22,272 elements), medium (61,725 elements), and fine (130,381 elements). We used a quadrilateral mesh shape (see Fig. 2-a). Fig. 2-b shows the locations explored in the independence tests. At points 1 to 5 marked in rear-wall, the local average velocity of water (u), turbulent kinetic energy (k), and dissipation rate (ϵ), were recorded. These values allow us to determine the shape of the velocity profile and how the nozzle geometry affects the flow field. The nozzle-wall shear stress distribution was measured along the green line. Values were recorded along the stage 1 and the stage 2 to find the ratio of circumferential velocity ($u_{\text{circumferential}}$) to the local average velocity (u).

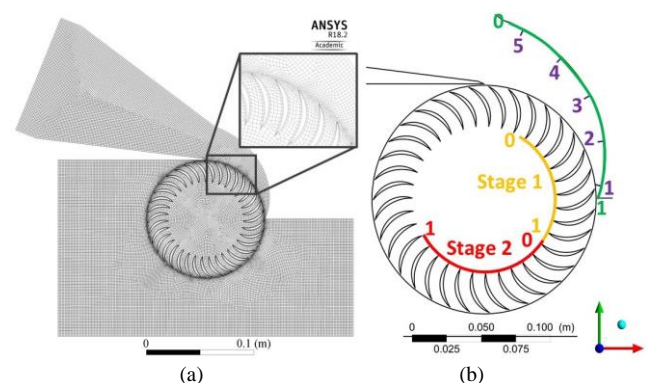


Fig. 2. Simulation process: (a) Visualization of mesh density; and (b) Locations of measurement.

Mesh and timestep independency was performed by comparing the torque (τ) of turbine. The GCI analysis was performed to report results of grid convergence studies and possibly provide an error value on the grid convergence of solution [23]. For example,

$$GCI_{12} = F_s \left| \frac{1}{\tau_{fine}} \frac{\tau_{medium} - \tau_{fine}}{r_{12}^{P_n} - 1} \right| \times 100\% \quad (7)$$

where F_s is a safety factor that was assigned the value of 1.25, and r is the grid refinement ratio:

$$r_{12} = \left(\frac{M_{finest}}{M_{finer}} \right)^{0.5} \quad (8)$$

where M is mesh number. Prior to GCI analysis, the order of convergence observed (P) was analysed using (9). Due to the calculation of (9) using the numerical method, The initial value for P_n was 2 and the calculations were iterated until the value of P stabilized [23].

$$P_{n+1} = \ln \left(\frac{\tau_{coarse} - \tau_{medium}}{\tau_{medium} - \tau_{fine}} (r_{12}^{P_n-1}) \right) + r_{12}^{P_n} / \ln(r_{12} \cdot r_{23}) \quad (9)$$

Besides, Richardson's extrapolation (τ_{exact}) was applied with the two finest resolutions to approximate the torque using (10) [23]:

$$\tau_{exact} = \tau_{fine} - \left(\frac{\tau_{medium} - \tau_{fine}}{r_{12}^{P_n+1} - 1} \right) \quad (10)$$

III. RESULTS

A. Verification and Validation of Simulation Setup

Before computing the simulations, independence testing using GCI was conducted. All the GCI analysis results for the number of mesh elements are given in Table 2. From Table 2, we find that 130,381 mesh elements are ideal for this study, with an error of 0.91% toward the exact value. This study used the GCI concept to provide errors for each timestep value and to determine the number of timesteps to be used. Table 3 gives the timestep independence test results using GCI with τ_{exact} . From Table 3, we chose the timestep frequency of 2500 Hz, with an error of 0.64%. These values can distinguish the confidence level of the data from the errors generated by computing ($<10\%$). Furthermore, when compared to previous studies [5] with the same conditions (see Fig. 3), the average error of the results was 2% for computational and 3% for experimental results, respectively. Thus, we validated that the timestep frequency of 2500 Hz and 130,381 mesh elements will yield an acceptable simulation.

B. Reynolds Number Effects

This study tested ten variations of the pressure inlet which

TABLE II
NUMBER OF ELEMENT INDEPENDENCE TEST RESULTS USING GCI ANALYSIS

Number of mesh	Normalized of spacing	τ (N·m)	r	P	GCI (%)
22272	2.42	241.19	-	-	-
61725	1.45	269.84	1.67	-	3.13
130381	1	274.58	1.45	3.25	0.91

TABLE III

TIMESTEP INDEPENDENCE TEST RESULTS USING GCI ANALYSIS					
Timestep frequency (Hz)	Normalized	τ (N·m)	r	P	GCI (%)
500	2.24	109.82	-	-	-
1250	1.41	118.62	1.58	-	2.24
2500	1	120.13	1.41	3.57	0.64

is represented as a Reynolds number (Re_c): $2.17 \times 10^6 \approx$ for 98.1 kPa; $3.06 \times 10^6 \approx$ 196.2 kPa; $3.75 \times 10^6 \approx$ 294.3 kPa; $4.33 \times 10^6 \approx$ 392.4 kPa; $4.48 \times 10^6 \approx$ 490 kPa; $5.31 \times 10^6 \approx$ 588.6 kPa; $5.73 \times 10^6 \approx$ 686.7 kPa; $6.13 \times 10^6 \approx$ 784.8 kPa; $6.50 \times 10^6 \approx$ 882.9 kPa; and $6.85 \times 10^6 \approx$ 981 kPa. The computational results for these variations are shown in Fig. 4. From Fig. 4, the peak efficiency is at the ratio of V_t/U (inlet velocity (V_t or W) per velocity of the runner (U)) of 1.8. This condition agrees with the findings of a previous study [1], [3], [5], [9], [24].

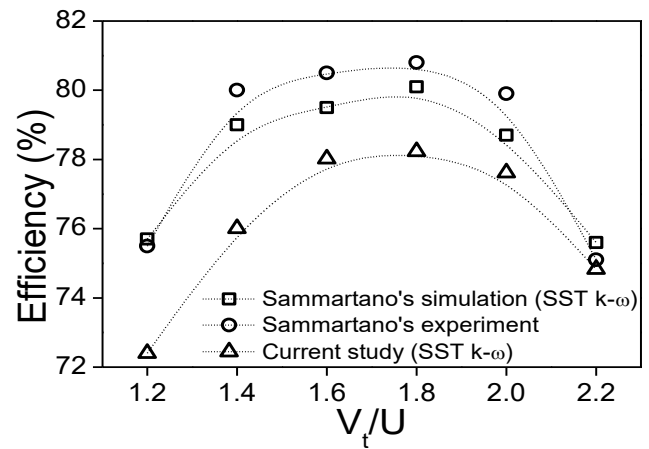


Fig. 3. Simulation results with previous study.

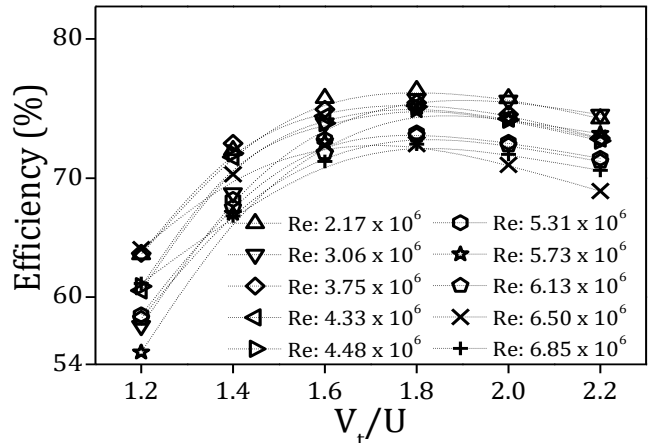


Fig. 4. Simulation results with variations Re_c .

IV. DISCUSSION

The flow patterns were studied to determine why converted water energy does not match expectations. Measurements are taken along the green line in Fig. 2-b shows that the centre of the rear wall has the lowest wall shear (τ_{wall}) value (see Fig. 5), which agrees with previously published results [18] in which the shape of the nozzle (height (S_0) and curvature) influenced changes in momentum. A nozzle with a greater curve radius at the rear

wall or S_o will have inlet velocity (W_1) with a tangential component, which will change the β_1 angle. Therefore, the energy conversion process in stage 1 does not match the expectations from the velocity triangle analysis. This behaviour can be anticipated if we analyse the relative dimensions of the inlet angle at stage 2 (β_3) equal to $((\alpha_2 + \beta_2))/2$. The computational results show that τ_{wall} is lower in the rear wall centre (at line 3 on Fig. 2-b) because the water velocity decreases even though the cross-sectional area of the flow field decreases. Furthermore, τ_{wall} is a function of the velocity gradient in the y-direction (u_j).

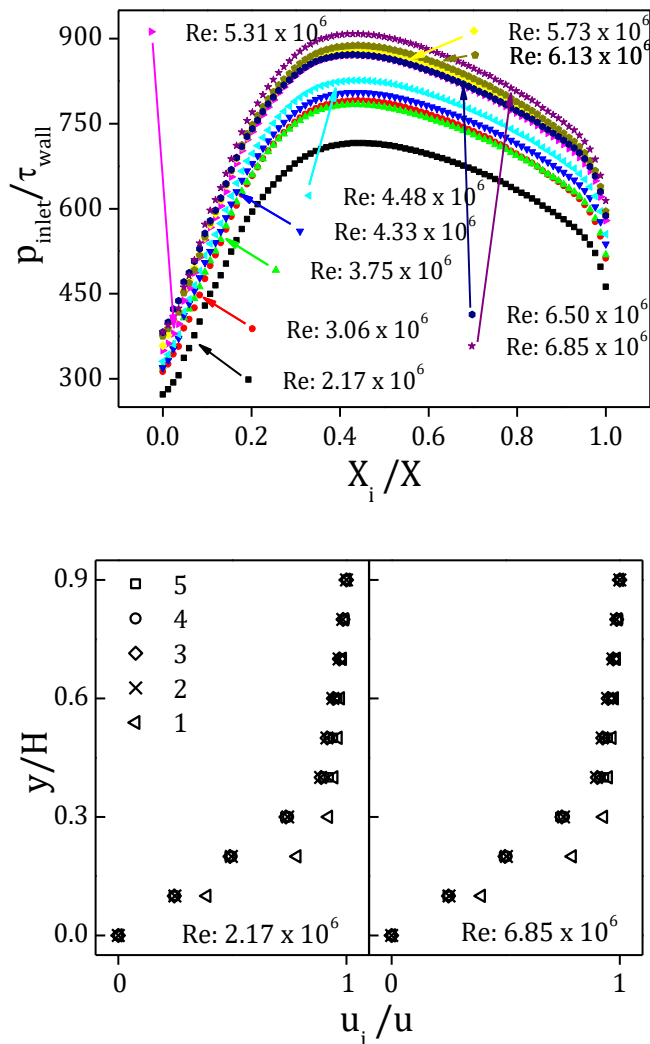


Fig. 6. Velocity profile in rear-wall

In Fig. 6, the Reynolds number (Re) used above is 10^6 in the fully turbulent flow category. If these conditions are compared to an exponential plot of the power-law velocity profile (n) against the Re , then the n values will range from 9 to 10. Consequently, the n value in this category is high, so that the flow in the nozzle is fully developed turbulent flow. The velocity profile is shown in rear-wall in Fig. 2-b also appears in Fig. 6. From Fig. 6, the highest n value is at location 1, close to the runner. This indicates that more-turbulent flow occurs when the water meets the runner. Moreover, the nozzle height (S_o) affects the performance of the CFT because the shape of the velocity profile follows the same pattern in all simulated conditions, so the percentage of momentum flux is also roughly constant.

Therefore, decreasing the nozzle height will not proportionally increase the water velocity and vice versa.

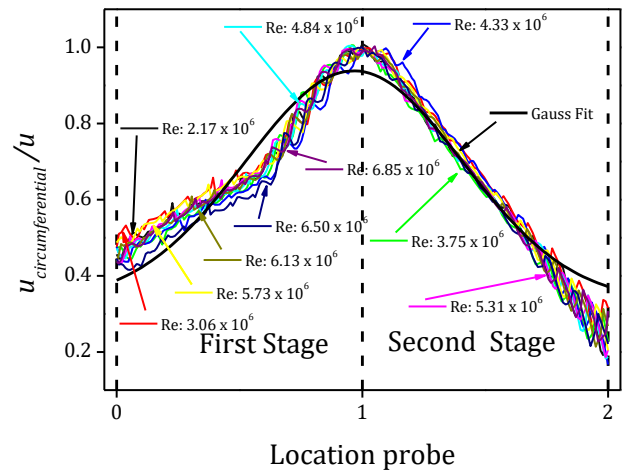


Fig. 7. The ratio of $u_{circumferential}/u$ at first and second stage

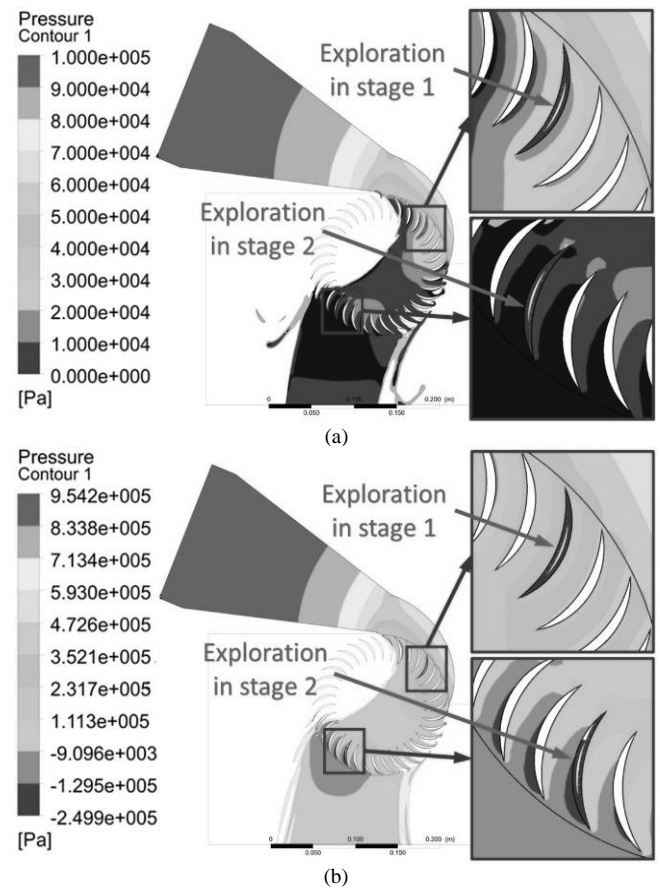


Fig. 8. Pressure contour of water at $V_r/U = 1.8$: (a) $Re: 2.17 \times 10^6$; (b) $Re: 6.85 \times 10^6$

The increasing momentum influences the water velocity and the mass flow, and the mass flow depends on the velocity profile. Turning to Fig. 6, $u_i/U = 0.99$ occurs at $y_i/y_{max} = 0.37$. Even though the nozzle height and water velocity vary between conditions, the momentum flux is constant. The momentum flux is constant because it is affected by the fluid viscosity, which depends on the velocity profile, and the velocity profile affects the thickness of the boundary layer [25]. Thus, the nozzle shape needs to be optimized to optimize turbine performance [18]. While

the shape of the velocity profile and the turbulent boundary layer thickness is known to affect the momentum flux of the flow, the results in Fig. 6 indicate that the highest water-momentum flux occurs only at the end of the nozzle, near the runner.

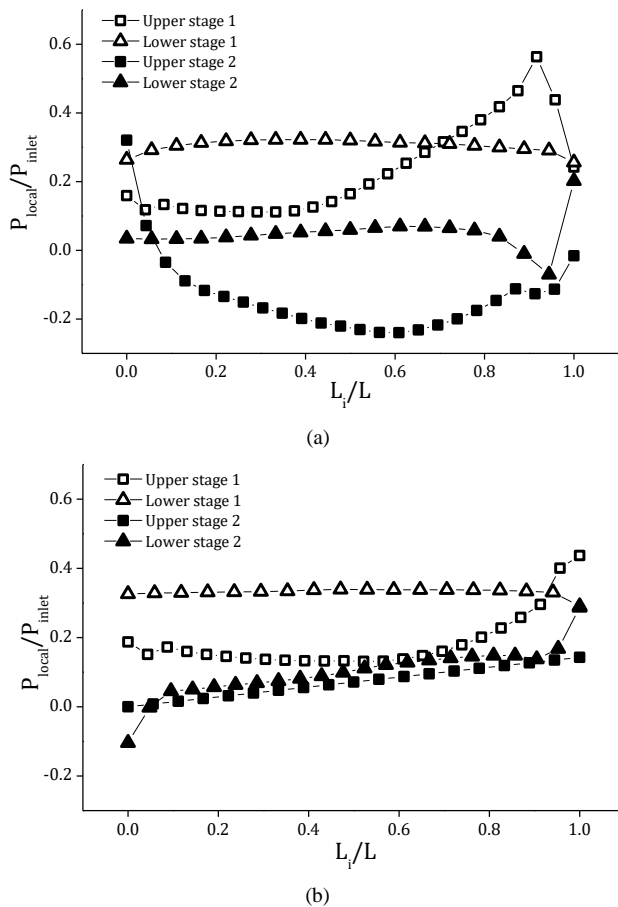


Fig. 9. Pressure distribution along the rear-wall line in Fig. 7: (a) Re: 2.17×10^6 ; (b) Re: 6.85×10^6

In Fig. 8, the lower parts of the blades have higher pressure than the upper part of the blades in both stage 1 and 2. This condition resembles the results in Fig. 9 and Fig. 12 in which the pressure on the top of the blade is less than the pressure on the lower part of the blade and the velocity of water on the lower part of the blade is higher than the velocity around the upper part of the blade, respectively. In other words, lift and drag forces affect the turbine's performance. However, these effects are not strong enough to prove that the CFT performance is also obtained from lift and drag force. Furthermore, in Fig. 9, the pressure gradient between the upper and lower parts of the blade at stage 2 is not significant. Consequently, the lift and drag forces do not have a significant effect on the energy conversion process of the CFT. Moreover, pressure drops on the upper parts of active blades occur because of the strong water momentum striking the lower part of the blade. Changes in momentum can be seen in Fig. 10, and are marked by the drop of water velocity flowing from the nozzle to stage 1, stage 2, and the outlet. These results confirm previous findings [1], [9] that classify the CFT as a type of impulse turbine that converts kinetic energy from flowing water.

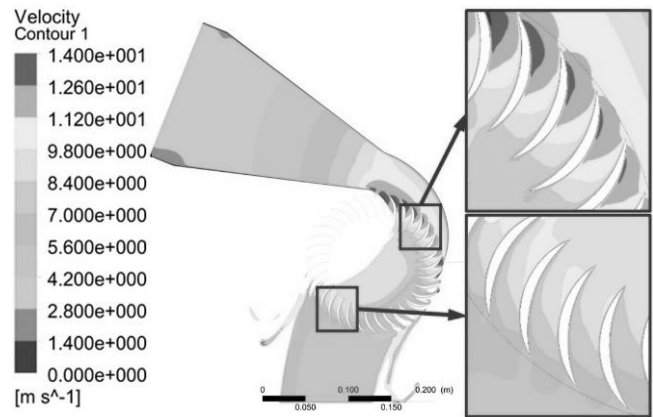


Fig. 10. Velocity contour of water at $V/U = 1.8$; for Re: 2.17×10^6

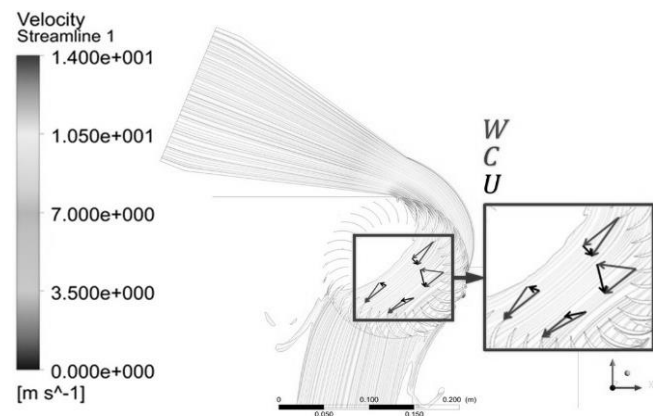


Fig. 11. Streamline velocity of water at $V/U = 1.8$; for Re: 2.17×10^6

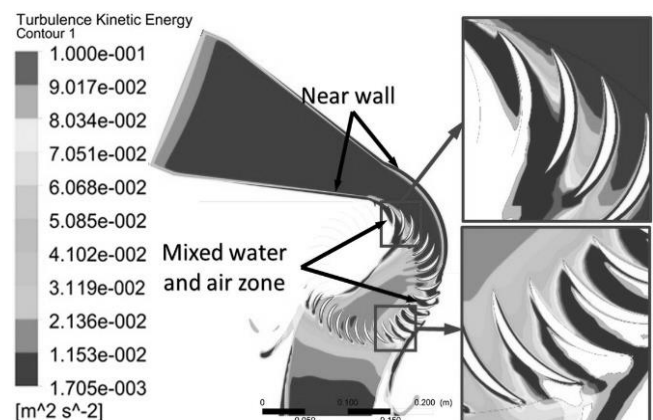


Fig. 12. Kinetic energy turbulent of water at $V/U = 1.8$; for Re: 2.17×10^6

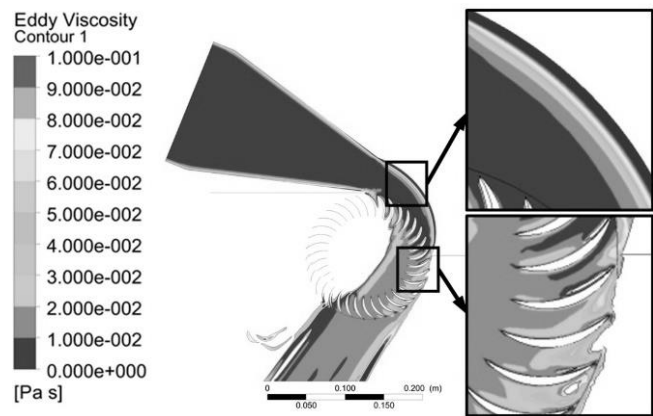


Fig. 13. Eddy viscosity contour of water at $V/U = 1.8$; for Re: 2.17×10^6

The turbulent kinetic energy ($k = 3(\overline{u'^2})/2$) is the sum of all the normal Reynolds stress ($\text{Re}_{\text{stress}}$) [27] and is a function of the velocity fluctuation or turbulent intensity (TI); u' also affects the $\text{Re}_{\text{stress}}$, see (4) [28]. $\text{Re}_{\text{stress}}$ comes from the interaction of velocity with vorticity [28]. Thus, changes in k will be proportional to $\text{Re}_{\text{stress}}$. In Fig. 12, zones with a high k value are near the wall and transition zones with mixed water and air. The near-wall has k higher than the far wall because the viscosity (μ) in this area is an important parameter while the density (ρ) is not [29]. However, in the mixture zone, density (ρ) is the important parameter [29]. For this reason, the VoF must be defined because it affects k and our ability to determine the density of the mixture. Figure 12 shows that the zone in which water mixes with air has higher $\text{Re}_{\text{stress}}$, which means that this region has less kinetic energy than the middle part of the flow.

Eddy viscosity or turbulent viscosity (μ_t) represents waves or mixing in the flow [28]. In Fig. 13, the eddy viscosity is more dominant around the wall of the nozzle, especially in the centre of the rear wall. This proves that mixing is not dominant in this region, and explains why the centre of the rear wall has the lowest shear wall (τ_{wall}).

V. CONCLUSION

Several parameters of the flow field in the CFT such as power-law velocity profile (n), turbulent kinetic energy (k), shear stress turbulent (τ_{shear}), shear wall (τ_{wall}), eddy viscosity or turbulent viscosity (μ_t), dissipation rate (ϵ) and Reynolds stress ($\text{Re}_{\text{stress}}$). The results are grouped into two categories: the nozzle and the runner. The nozzle, at $\text{Re}: 2.17 \times 10^6$ to 6.85×10^6 , is the shape of the velocity profile expressed by the power-law velocity profile (n). n at the entrance (points 5, 4, 3 and 2) is 9; while at the exit of the nozzle (point 1), it is 10. The shear wall (τ_{wall}) distribution is highest at the base and tip of the nozzle; it is lowest at the centre. The eddy or turbulent viscosity (μ_t) is more dominant in the wall of the nozzle, especially at the centre of the rear wall. This proves that wave mixing is no longer dominant at this point, and explains how the rear wall has the lowest τ_{wall} . The eddy or turbulent viscosity (μ_t) profile at the nozzle is proportional to the turbulent kinetic energy (k), the turbulent boundary layer profile (δ_t), and $\text{Re}_{\text{stress}}$. Furthermore, the highest turbulent kinetic energy (k), dissipation rate (ϵ) and Reynolds stress ($\text{Re}_{\text{stress}}$) are located at the runner. This finding indicates that the nozzle shape affects the momentum flux (performance of the CFT). Good nozzle geometry can transfer the maximum water energy into the blade. This can be achieved by discharge and direction, optimizing velocity magnitude. This minimizes energy loss due to friction between the stream (τ_{wall} and τ_{turb}), vortex (k and ϵ) and the mass of wasted fluid. Second, on the runner, the highest turbulent kinetic energy (k), dissipation rate (ϵ) and Reynolds stress ($\text{Re}_{\text{stress}}$) are located at the runner. Not all the water's energy converted into mechanic energy because some of that energy is lost to mixing between water and air. The lift force on the active blades is not established by the flow field that crosses the

upper part of the blade, but instead comes from the momentum of water that strikes the lower part of the blade. A vortex or reverse current is formed from the separation of the flow from the blade. The vortex causes β_2 is not 90° so changes the \vec{C}_2 and \vec{W}_2 affect the magnitude of \vec{U} . The β_2 is not 90° occur along with the outlet of stage 2 so that magnitude of \vec{U} is non-uniform impact runner rotation is not normal. This affects the runner's performance more than the rotational flow of air in the CFTs.

The main challenge in implementing the CFTs in remote areas lies in simplifying the turbine shape to cut costs. Our future work will include the design of a simple shape that will allow easy manufacturing, operation, and maintenance. Because remote areas often have low income, cost-effectiveness must be considered in the design of small-scale independent distributed power plants.

REFERENCES

- [1] D. Adanta, R. Hindami, Budiarso, Warjito, and A. I. Siswantara, "Blade Depth Investigation on Cross-Flow Turbine by Numerical Method," in *2018 4th International Conference on Science and Technology (ICST)*, 2018, pp. 1–6.
- [2] Budiarso, Warjito, M. N. Lubis, and D. Adanta, "Performance of a Low Cost Spoon-Based Turgo Turbine for Pico Hydro Installation," *Energy Procedia*, vol. 156, pp. 447–451, 2019.
- [3] A. I. Siswantara, Budiarso, A. P. Prakoso, G. G. R. Gunadi, Warjito, and D. Adanta, "Assessment of Turbulence Model for Cross-Flow Pico Hydro Turbine Numerical Simulation," *CFD Letters*, vol. 10, pp. 38–48, 2018.
- [4] B. Ho-Yan, "Design of a Low Head Pico Hydro Turbine for Rural Electrification in Cameroon," University of Guelph, 2012.
- [5] V. Sammartano, G. Morreale, M. Sinagra, and T. Tucciarelli, "Numerical and Experimental Investigation of a Cross-Flow Water Turbine," *Journal of Hydraulic Research*, vol. 54, no. 3, pp. 321–331, 2016.
- [6] R. Montanari, "Criteria for the Economic Planning of a Low Power Hydroelectric Plant," *Renewable energy*, vol. 28, no. 13, pp. 2129–2145, 2003.
- [7] J. De Andrade *et al.*, "Numerical Investigation of the Internal Flow in a Banki Turbine," *International Journal of Rotating Machinery*, vol. 2011, 2011, doi: <https://doi.org/10.1155/2011/841214>.
- [8] M. Sinagra, V. Sammartano, C. Aricò, and A. Collura, "Experimental and Numerical Analysis of a Cross-Flow Turbine," *Journal of Hydraulic Engineering*, vol. 142, no. 1, p. 4015040, 2015.
- [9] D. Adanta, Budiarso, Warjito, A. I. Siswantara, and A. P. Prakoso, "Performance Comparison of NACA 6509 and 6712 on Pico Hydro Type Cross-Flow Turbine by Numerical Method," *Journal of Advanced Research in Fluid Mechanics and Thermal Sciences*, vol. 45, pp. 116–127, 2018.
- [10] R. C. Adhikari and D. H. Wood, "Computational Analysis of Part-Load Flow Control for Crossflow Hydro-Turbines," *Energy for Sustainable Development*, vol. 45, pp. 38–45, 2018.
- [11] Ram C. Adhikari, "Design Improvement of Crossflow Hydro Turbine." University of Calgary, 2016.
- [12] W. W. Durgin and W. K. Fay, "Some Fluid Flow Characteristics of a Cross-Flow Type Hydraulic Turbine," *Small Hydro Power Fluid Machinery*, pp. p77-83, 1984.
- [13] S. Chichkhede, V. Verma, V. K. Gaba, and S. Bhowmick, "A Simulation Based Study of Flow Velocities across Cross Flow Turbine at Different Nozzle Openings," *Procedia Technology*, vol. 25, pp. 974–981, 2016.
- [14] H. G. S. Totapally and N. M. Aziz, "Refinement of Cross-Flow Turbine Design Parameters," *Journal of energy engineering*, vol. 120, no. 3, pp. 133–147, 1994.
- [15] S. Khosrowpanah, A. A. Fiuzat, and M. L. Albertson, "Experimental Study of Cross-Flow Turbine," *Journal of Hydraulic Engineering*, vol. 114, no. 3, pp. 299–314, 1988.
- [16] M. Kaniecki and J. Steller, "Flow Analysis through a Reaction Cross-Flow Turbine," in *Proceedings of Conference on modelling fluid flow CMFF*, 2003, vol. 3, pp. 2003–2006.
- [17] V. Sammartano, G. Morreale, M. Sinagra, A. Collura, and T.

- Tucciarelli, "Experimental Study of Cross-Flow Micro-Turbines for Aqueduct Energy Recovery," *Procedia Engineering*, vol. 89, pp. 540–547, 2014.
- [18] Y.-D. Choi, J.-I. Lim, Y.-T. Kim, and Y.-H. Lee, "Performance and Internal Flow Characteristics of a Cross-Flow Hydro Turbine by the Shapes of Nozzle and Runner Blade," *Journal of fluid science and technology*, vol. 3, no. 3, pp. 398–409, 2008.
- [19] V. Sannarath, C. Aricò, A. Carravetta, O. Fecarotta, and T. Tucciarelli, "Banki-Michell Optimal Design by Computational Fluid Dynamics Testing and Hydrodynamic Analysis," *Energies*, vol. 6, no. 5, pp. 2362–2385, 2013.
- [20] A. Fluent, "Ansys Fluent Theory Guide," *ANSYS Inc, USA*, vol. 15317, pp. 724–746, 2011.
- [21] Florian R. Menter, "Zonal Two Equation Kw Turbulence Models for Aerodynamic Flows," in *23rd fluid dynamics, plasmadynamics, and lasers conference*, 1993, p. 2906.
- [22] F. R. Menter, "Two-Equation Eddy-Viscosity Turbulence Models for Engineering Applications," *AIAA journal*, vol. 32, no. 8, pp. 1598–1605, 1994.
- [23] P. J. Roache, *Verification and validation in computational science and engineering*. Hermosa, 1998.
- [24] A. P. Prakoso, Warjito, A. I. Siswantara, Budiarmo, and D. Adanta, "Comparison Between 6-DOF UDF and Moving Mesh Approaches in CFD Methods for Predicting Cross-Flow Pico- Hydro Turbine Performance," *CFD Letters*, vol. 11, no. 6, pp. 86–96, 2019.
- [25] T. Cebeci, *Analysis of turbulent boundary layers*, vol. 15. Elsevier, 2012.
- [26] R. C. Adhikari and D. H. Wood, "A New Nozzle Design Methodology for High Efficiency Crossflow Hydro Turbines," *Energy for Sustainable Development*, vol. 41, 2017, doi: 10.1016/j.esd.2017.09.004.
- [27] L. Davidson, *Fluid mechanics, turbulent flow and turbulence modeling*. Chalmers University of Technology, 2015.
- [28] H. Tennekes and J. L. Lumley, *A first course in turbulence*. MIT press, 1972.
- [29] B. R. Munson, T. H. Okiishi, W. W. Huebsch, and A. P. Rothmayer, *Fluid mechanics*. Wiley Singapore, 2013.

Fluid Mechanics and Thermal Science; Energy Reports, Journal Mechanical Engineering and Science; and several seminar proceedings.



Dendy Adanta was born in South Sumatera, Indonesia at June 5th 1993. Degree: M.Eng. (2017) in Mechanical Engineering from Universitas Indonesia, Jakarta-Indonesia. Dr. (2020) in Mechanical Engineering, Universitas Indonesia, Indonesia.

He has work as lecture at Universitas Sriwijaya, South Sumatera, Indonesia. Dr. Dendy Adanta, M.Eng. some publication had written to the International Journal of Technology; International Journal on Advanced Science, Engineering and Information Technology; CFD Letters; Journal of Advanced Research in Fluid Mechanics and Thermal Science; Energy Reports; Journal of Mechanical Engineering and Sciences; and several seminar proceedings

Dr. Dendy Adanta, M.Eng. is memberships in professional societies in the IAENG.



Warjito was born in Cilacap, Indonesia at August 8th 1963. Degree: Ir (1988) in Mechanical Engineering from Universitas Indonesia, Jakarta-Indonesia M. Eng. (1998) from Mechanical Science Hokkaido University, Sapporo Japan. PhD (2001) from Mechanical Science Hokkaido University, Sapporo-Japan. Major Field of study is fluid dynamics.

He has work at oil and gas production facilities fabricator after graduated from University of Indonesia for 3 years, after which he joined the laboratory of fluid mechanics Mechanical Engineering until now. Prof. Ir. Warjito M.Eng., PhD. have some of publication had written to the Journal of Experimental in Fluid; Applied Mechanic and Material; International Journal of Technology; International Journal of Fluid Mechanic Research; International Journal on Advanced Science, Engineering and Information Technology; CFD Letters; Journal of Advanced Research in Fluid Mechanics and Thermal Science; International Review of Mechanic Research; International Review of Mechanical Engineering; Energy Reports, Journal Mechanical Engineering and Science; and several seminar proceedings.



Budiarmo was born in Yogyakarta, Indonesia at March 23rd 1950. Degree: Ir (1977) in Mechanical Engineering, Universitas Indonesia, Indonesia. M. Eng. (1996) in Mechanical Engineering, National University of Singapore (NUS), Singapore. Dr. (2005) in Mechanical Engineering, Universitas Indonesia, Indonesia.

He has work in Universitas Indonesia as a Lecture and joined the laboratory of fluid mechanics Mechanical Engineering until now. Prof. Dr. Ir. Budiarmo, M.Eng. some publication has written to Journal of Mechanical Science and Technology; International Journal of Mechanical and Mechanics Engineering; International Journal of Fluid Mechanics Research; International Review of Mechanical Engineering; ARPN Journal of Engineering and Applied Science; International Journal of Technology; International Review of Aerospace Engineering; CFD Letters; International Journal on Advanced Science, Engineering and Information Technology; Journal of Advanced Research in